Harnessing Fe 2 O 3 to Improve HAP Composites: Investigating Radiation Shielding, Mechanical Attributes, and Magnetic Field Effects

Roya Boodaghi Malidarre (roya_boodaghi@yahoo.com)
Payame Noor University
Iskender Akkurt
Suleyman Demirel University
Hesham M.H. Zakaly
Al-Azhar University
Abdul Vahap Korkmaz
Afyonkocatepe University
Ismail Ekmekci
Istanbul Ticaret University

Research Article

Keywords: HAP Bio-composite, FLUKA Environment, Magnetic Field

Posted Date: June 7th, 2023

DOI: https://doi.org/10.21203/rs.3.rs-3024124/v1

Additional Declarations: No competing interests reported.

Abstract

Hydroxyapatite (HAP) bio-composites are widely utilized for the repair and replacement of bone and teeth tissues in humans. However, due to their suboptimal mechanical properties, the strength and durability of pure HAP have been improved by incorporating various alloys and materials. This study examines the radiation shielding and mechanical properties of Fe_2O_3-reinforced HAP composites for use as implants, with Fe_2O_3 concentrations of 0.0, 2.5, 5.0, and 7.5 wt.%. The study also investigates the composite's behavior in a magnetic field. Using the FLUKA Monte Carlo Code, radiation shielding factors are determined, and the mechanical properties of the composites are assessed through theoretical methods. Results indicate that increasing Fe_2O_3 content in HAP bio-composites enhances the radiation shielding and mechanical properties of the selected samples. Additionally, without a magnetic field, particle distribution displays symmetry along the x-axis; however, when exposed to a magnetic field of Bx=5 microT, a distinct pattern emerges.

1. Introduction

Hydroxyapatite (calcium phosphates, $Ca_{10}(PO_4)_6(OH)_2$, HAP) is a hydroxyl end member of the Apatite group. This is characterized by its ionic substitution capability which makes it ideal for medical applications. The close resemblance of HAP to bones and teeth makes this material useful as an implant for dental and orthopedic applications [1–3]. Because of the HAP's poor mechanical qualities, significant improvements are achieved by adding various dopants like ZnO, ZrO_2, Fe_3O_4, and Li to HAP [1–16]. Htun et al. [2] discovered that reinforced CaO-ZrO_2/HAP is an effective material for improving the strength and toughness of the selected bio-composites. The reinforced ZrO_2/HAP strength has been effectively improved from 35.70 MPa to 52.88 MPa, and the toughness has been increased from 0.65 MPa.m $^{1/2}$ to 1.33 MPa.m $^{1/2}$. They also discovered that adding CaF_2 to CaO-ZrO_2/HAP improves the bio-composites' sinterability. On the other hand, because HAP bio-composites are widely used in the human body, having information about the interactions of gamma rays with patients via radiotherapy or other radiation examinations is critical. Accordingly, the current work investigates gamma photons penetration in HAP + Fe_2O_3 as derived from the Beer-Lambert Law. Other researchers have noticed this issue recently [17–18]. H. Badran et. al. [17] reported the lithium-doped hydroxyapatite nano-composites' gamma attenuation coefficient and dielectric features. Composites were prepared using the sol-gel technique. Outcomes reveal that the gamma attenuation coefficient values increased from 0.562 cm^{-1} for 0.0 wt.% Li-HAp to 2.190 cm^{-1} for 40.0 wt.% Li-Hap. In addition, the Li concentration affected the dielectric values and proved that the synthesized nano-composite are ideal material for medical purposes. Another integral item to consider is the HAP + Fe_2O_3 composite response in the magnetic field. The interactions of gamma photons with sample and lead shields produce a huge number of charged particles that are impacted in the presence of the magnetic field [19].

Thus, the current study investigates radiation shielding qualities, mechanical properties, and HAP + Fe_2O_3 reaction in the magnetic field. To acquire the attenuation performance, simulations are performed in the

FLUKA Monte Carlo Code environment. Mechanical properties are extracted and the outcomes are presented utilizing Makishima and Mackenzie theory. In addition, the particles' spatial map in the absence and presence of a magnetic field is examined.

2. Materials and Methods

2.1 Composites Preparation

In the current study, Fe_2O_3 is doped with HAP bio-composites in concentrations of 0.0, 2.5, 5.0, and 7.5 wt.%, and four unique samples denoted as S1, S2, S3, and S4 are simulated. Table 1 gives the approved composites' weight percentages (wt.%) and chemical compositions. The samples are irradiated for wide energy spans between 0.01 and 15 MeV.

Table 1
The wt. % of the HAP + Fe_2O_3 composite.

Composites codes	wt.% of the compositions	Density ($g.cm^{-3}$)
S1	100.0%HAP + 0.0%Fe_2O_3	3.14
S2	97.5%HAP + 2.5% Fe_2O_3	3.17
S3	95.0%HAP + 5.0% Fe_2O_3	3.20
S4	92.5%HAP + 7.5% Fe_2O_3	3.24

2.2 FLUKA Monte Carlo Code Environment

FLUKA is an important and widely used Monte Carlo code for different applications [20]. Thus besides other code it has been in a variety of studies in radiation fields [21–39]. In the present study, the FLUKA Monte Carlo Code is utilized to calculate the radiation shielding capacity of the HAP + Fe_2O_3 samples [18, 40–41]. The BEAM card defines the isotropic source in this code. The position and direction of the 1 cm radius gamma photon source are controlled by a BEAMPOS card. The sample is modeled as a cylinder (RCC) with a thickness of 2 cm and a height of 10 cm. The BLKBODY shell with an inner radius of 1000 cm and an outside radius of 1010 cm encases the 3 cm radius simulated lead collimators, source, and sample. GEOBEGIN and GEOEND cards specify all geometries. MATERIAL and COMPOUNDS cards are used to model samples' density, elemental fractions, and weight percentages.

2.3Radiation Shielding Capacity

Linear Attenuation Coefficient (LAC) is utilized to predict the gamma photon attenuation features through Beer-Lambert Law (BLL) [42–53]:

$$\mathbf{I} = \mathbf{I}_0 . \mathbf{e}^{-\mathbf{LAC}*\mathbf{a}} \quad (1)$$

Where I_0 and I are the initial and final intensities respectively, and a is the thickness of the preferred samples. Half Value Layer (HVL) and Tenth Value Layer (TVL) play a significant role to discover the attenuation qualities of different materials derived through the following Eqs. [53–55]:

$$\mathrm{HVL\,(cm)} = \frac{\mathrm{Ln\,(2)}}{\mathrm{LAC\,(cm^{-1})}} (2)$$

$$\mathrm{TVL\,(cm)} = \frac{\mathrm{Ln\,(10)}}{\mathrm{LAC\,(cm^{-1})}} (3)$$

2.4 Mechanical Properties of the HAP + Fe_2O_3 Composites

Makishima and Mackenzie Model (MMM) [56–58] is used to obtain the mechanical features of the HAP + Fe_2O_3 via Eqs. 4–12. The bond dissociation energy (G_t, kJ.cm^{-3}) and the packing factor (V_i, cm^3.mol^{-1}) of the investigated composites are employed to derive the mechanical properties such as packing density (V_t, cm^3.mol^{-1}), Young's modulus (E, GPa), Bulk modulus (B, GPa), Shear modulus (S, GPa), Longitudinal modulus (L, GPa), Poisson's ratio (σ), and Indentation modulus (E*, GPa):

$$\mathrm{G_t(kJ.\,cm^{-3})} = \sum_i \mathrm{G_i x_i}\,(4)$$

$$\mathrm{V_i\left(cm^3.\,mol\right)} = \frac{4\pi}{3}\mathrm{N_A}\left(\mathrm{XR_A^3} + \mathrm{YR_o^3}\right)(5)$$

$$\mathrm{V_t\left(cm^3.\,mol\right)} = \frac{\rho}{\mathrm{M}}\sum_i \mathrm{V_i x_i}\,(6)$$

$$\mathrm{E\,(GPa)} = 8.36\mathrm{V_t G_t}\,(7)$$

$$\mathrm{B\,(GPa)} = 10\mathrm{V_t^2 G_t}\,(8)$$

$$\mathrm{S\,(GPa)} = \frac{30\mathrm{V_t^2 G_t}}{(10.2\mathrm{V_t} - 1)} (9)$$

$$\mathrm{L\,(GPa)} = \mathrm{B} + \frac{4}{3}\mathrm{S}\,(10)$$

$$\sigma = 0.5 - \frac{1}{7.2\mathrm{V_t}} (11)$$

$$\mathrm{E^*} = \frac{\mathrm{E}}{1-\sigma^2} (12)$$

Where N_A, R_A, R_O, X, and Y represent Avogadro's number, ionic radius of the metal, ionic radius of oxygen, the number of metal atoms, and the number of oxygen atoms, respectively [59–61].

2.5 HAP + Fe_2O_3 Composite Response in a Magnetic Field

A huge number of charged particles are produced when gamma photons interact with composite materials. In the presence of a magnetic field, these particles react differently in various composites. Accordingly, to assess the trend of charged particles in the preferred composite, a magnetic field with the value of 5 microT in the x-axis (B_x=5 microT) is applied to the HAP + Fe_2O_3 composite, and the charged particle behavior is examined.

3. Results and Discussion

The Half Value Layer (HVL) is an important measure for estimating the attenuation properties of different samples. The HVL for four S sample types, S1, S2, S3, and S4 is calculated, and the results are visually depicted in Fig. 2. HVL is energy-dependent in low and intermediate energy zones, increasing as energy is increased. But, in the high-energy region, the HVL varies with log E [62–65]. In addition, increasing the rate of Fe_2O_3 in HAP samples results in decreased HVL, and less thickness of S samples is necessary to reduce the initial intensity to half of it. Some numerical results are provided to back up this argument. The HVL values for recommended samples vary between 0.019 and 9.994 cm, 0.018 and 9.832 cm, 0.017 and 9.674 cm, 0.016 and 9.508 cm for 0.01 to 15 MeV, from S1 to S4, respectively. Thus, the S4 sample with the highest concentration of Fe_2O_3 possesses the lowest HVL value in all energy ranges and performs better in terms of gamma photon protection. The Tenth Value Layer (TVL) versus Fe_2O_3 concertation in HAP composites is presented in Fig. 3 for energy levels of 0.1, 0.6, 4.0, 6.0, and 15 MeV. As shown, increasing the rate of Fe_2O_3 in HAP samples leads TVL to fall to lower values. However, the reduction in the high-energy zone is significant when compared to low-energy levels. For example, at 0.1 MeV, TVL ranges from 3.846 to 3.580 cm, whereas at 15 MeV, TVL ranges from 33.201 to 31.190 cm for S1 to S4 samples. Furthermore, the results show that increasing the energy in a specified S sample from 0.1 to 15 MeV increases TVL.

It is beneficial to analyze mechanical moduli in order to evaluate the effectiveness of preferred composites in various technologies. Thus, in the current work, E, B, S, L, Poisson's ratio, and E* are theoretically estimated. Increasing the rate of the Fe_2O_3 in HAP samples raises the E, B, S, and L from 391.13 to 520.17 GPa, 357.18 to 677.18 GPa, 148.43 to 189.57 GPa, and 468.51 to 819.36 GPa, respectively. E* follows a similar pattern. That is, E* is proportional to the concentration of Fe_2O_3. Furthermore, as expected, mechanical moduli variations behave similarly to changes in V_t, [66–68] which ranges from 0.76 to 1.08 $m^3.mol^{-1}$ for S1 to S4 samples. On the other hand, Poisson's ratio acts opposite to other mechanical parameters, and a considerable reduction in Poisson's ratio is detected for S1 to S4 samples. The mechanical moduli versus bond dissociation energy (G_t) show that increasing the rate of

Fe_2O_3 in HAP samples reduces the G_t from 256.98 to 239.74 $kJ.cm^{-3}$, which may be attributed to replacing low G_t material (Fe_2O_3) with high G_t material (HAP) in the provided samples.

To determine why mechanical moduli increase from S1 to S4 samples, E, B, S, L, Poisson's ratio, and E* are plotted versus density in Figs. 8, 9. A strong link exists between density and mechanical moduli except for Poisson's ratio. That is, increasing the sample density from S1 with the density of $\rho = 3.14$ $g.cm^{-3}$ to S4 with the density of $\rho = 3.24$ $g.cm^{-3}$ induces a dramatic increase in mechanical moduli. This could be related to an increase in the stiffness of the samples, which improves the mechanical properties significantly [67, 68]. The results obtained in this work are in consist on previous data in the literature [69-]

In order to evaluate the Fe_2O_3 response in the magnetic field, two separate cases are studied in Figs. 10 and 11: In the absence of magnetic field and in the presence of magnetic field with the value of B_x=5 microT. According to Fig. 10 (in the absence of a magnetic field case), the particles' spatial map exhibits symmetric behavior along the x-axis, but Fig. 11 (in the presence of magnetic field along the x-axis with the value Bx = 5 microT) exhibits different behavior. That is, in the presence of a magnetic field, no symmetry is observed. This trend demonstrates that Fe_2O_3 is an effective magnetic shield.

4. Conclusion

The current work looks into the radiation shielding quality, mechanical characteristics, and Fe_2O_3 response in a magnetic field. To determine the gamma photons shielding capability of the selected HAP composite samples, the FLUKA environment is used. Because the Hap bio-composite is used as an implant, the mechanical properties of the chosen composite are also assessed. The charged particles' spatial maps are evaluated in two different cases. Outcomes show that

- Increasing the rate of the Fe_2O_3 in HAP samples improves the attenuation features of the S samples.
- A strong relationship between density and mechanical moduli related to the S samples is monitored.
- By increasing the Fe_2O_3 concentration from S1 to S4 sample, G_t decreases rapidly.
- Particles' spatial map exhibits symmetric behavior along the x-axis in the absence of the magnetic field, while a different trend is monitored in the presence of the magnetic field.

Declarations

Availability of data and materials: All data are added to the paper.

Conflict of Interest: The authors declare that they have no conflict of interest.

Funding: This paper is not supported by any company.

Acknowledgments: Not Applicable

Authors' contributions: Not Applicable.

Ethics approval: Not applicable.

Consent to participate: Not Applicable.

Consent for publication: Not Applicable.

References

1. Qiu, H., Yang, J., Kodali, P., Koh, J., Ameer, G. A., 2006. A citric acid-based hydroxyapatite composite for orthopedic implants, Biomat. 27, 5845–5854.
2. Htun, Z. L., Ahmad, N., Thant, A. A., Noor, A. F. M., 2016. Characterization of CaO-ZrO_2 Reinforced Hap Biocomposite for Strength and Toughness Improvement, Procedia Chem. 19, 510 – 516.
3. Koksal, O. K., Tozar, A., Cengiz,E., Karahan, I. H., Apaydin,G., 2020. A research on the Gamma Ray Attenuation Characteristics for Real Bone and Manganese Substituted Artificial Bone Dust, Cumhuriyet Sci. J., 41, 85-92.
4. Jarcho, M., Kay, J.F., Gumaer, K.I., Doremus, R.H., Drobeck, H. P., 1997. Tissue, cellular and Subcellular Events at a Bone-Ceramic Hydroxylapatite Interface. J. Bioeng. 1, 79–92.
5. Nayak, A.K., 2010. Hydroxyapatite Synthesis Methodologies: An Overview. Int. J. Chem. Tech. Res. 2, 903–7.
6. Wang, X., 2011. Preparation of Magnetic Hydroxyapatite and Their Use as Recyclable Adsorbent for Phenol in Wastewater, Clean – Soil, Air, Water, 39, 13–20.
7. Waheed, F. , İmamoğlu, M. , Karpuz, N. & Ovalıoğlu, H. (2022). Simulation of Neutrons Shielding Properties for Some Medical Materials . International Journal of Computational and Experimental Science and Engineering , 8 (1) , 5-8 . DOI: 10.22399/ijcesen.1032359
8. [8]Çilli, A. , Beken, M. & Kurt, N. (2022). Determination of Theoretical Fracture Criteria of Layered Elastic Composite Material by ANFIS Method from Artificial Intelligence . International Journal of Computational and Experimental Science and Engineering , 8 (2) , 32-39 . DOI: 10.22399/ijcesen.1077328
9. Arslankaya, S. & Çelik, M. T. (2021). Prediction of Heart Attack Using Fuzzy Logic Method and Determination of Factors Affecting Heart Attacks . International Journal of Computational and Experimental Science and Engineering , 7 (1) , 1-8 . DOI: 10.22399/ijcesen.837731
10. İskender AKKURT, N. Ayten UYANIK, Kadir GÜNOĞLU “Radiation dose Estimation: An in vitro Measurement for Isparta-Turkey” International Journal of Computational and Experimental Science and Engineering 1-1(2015)1-4 DOI: 10.22399/ijcesen.194376
11. Demir, N., Tarim, U.A., Popovici, MA. et al. Investigation of mass attenuation coefficients of water, concrete and bakelite at different energies using the FLUKA Monte Carlo code. J Radioanal Nucl Chem 298, 1303–1307 (2013). https://doi.org/10.1007/s10967-013-2494-y

12. Akkurt, I., Al-Obaidi, S., Akyildirim, H. et al. Neutron Shielding for 252Cf Source: FLUKA Simulations and Measurements. Iran J Sci Technol Trans Sci (2022). https://doi.org/10.1007/s40995-022-01318-1
13. Boodaghi Malidarre, R. , Akkurt, İ. , Gunoglu, K. & Akyıldırım, H. (2021). Fast Neutrons Shielding Properties for HAP-Fe2O3 Composite Materials . International Journal of Computational and Experimental Science and Engineering , 7 (3) , 143-145 . DOI: 10.22399/ijcesen.1012039
14. Salima, B., Seloua, D., Djamel, F. & Samir, M. (2022). Structure of pumpkin pectin and its effect on its technological properties. Applied Rheology, 32(1), 34-55. https://doi.org/10.1515/arh-2022-0124
15. Karaali, Rabi and Keven, Arzu. "Evaluation of four different cogeneration cycles by using some criteria" Applied Rheology, vol. 32, no. 1, 2022, pp. 122-137. https://doi.org/10.1515/arh-2022-0128
16. Şen Baykal, D , Tekin, H , Çakırlı Mutlu, R . (2021). An Investigation on Radiation Shielding Properties of Borosilicate Glass Systems . International Journal of Computational and Experimental Science and Engineering , 7 (2) , 99-108 . DOI: 10.22399/ijcesen.960151
17. Badran, H., Yahia, I.S., Hamdy, M.S., Awwad, N.S. 2017. Lithium-doped Hydroxyapatite Nano-composites: Synthesis, Characterization Gamma Attenuation Coefficient and Dielectric Properties. Radiat. Phy. Chem. 130, 85–91. httpt://doi.org/10.1016/j.rad phys. chem.2016.08.001.
18. Boodaghi Malidarre, R., Akkurt, I., Boodaghi Malidarreh, P., Arslankaya, S., 2022 Investigation and ANN-based Prediction of the Radiation Shielding, Structural and Mechanical Properties of the Hydroxyapatite (HAP) Bio-Composite as Artificial Bone, Radiat. Phys. Chem. 197, 110208.
19. Ghasemi, f., shahriari, m., & abbasi davani, f.. (2012). investigation of charged particle transport in magnetic field and simulation of synchrotron radiation by fluka. journal of nuclear science and technology, -(1 (59)), 8-14. sid. https://sid.ir/paper/97572/en
20. G.Battistoni, T. Boehlen, F. Cerutti, P.W. Chin, L.S. Esposito, A. Fassò, A. Ferrari, A. Lechner, A. Empl, A. Mairani, A. Mereghetti, P. Garcia Ortega, J. Ranft, S. Roesler, P.R. Sala, V. Vlachoudis, G. Smirnov,"Overview of the FLUKA code", Annals of Nuclear Energy 82, 10-18 (2015).
21. RB Malidarre, I Akkurt, O Kocar, I Ekmekci, Analysis of radiation shielding, physical and optical qualities of various rare earth dopants on barium tellurite glasses: A comparative study, Radiation Physics and Chemistry, 110823.
22. A Sengul, MS Akhtar, I Akkurt, RB Malidarre, Z Er, I Ekmekci, Gamma-neutron shielding parameters of (S3Sb2) x (S2Ge) 100− x chalcogenide glasses nanocomposite, Radiation Physics and Chemistry 204, 110675.
23. Arbouz, H. (2022). Modeling of a Tandem Solar Cell Structure Based on CZTS and CZTSe Absorber Materials . International Journal of Computational and Experimental Science and Engineering , 8 (1) , 14-18 . DOI: 10.22399/ijcesen.843038
24. Rwashdı, Q. A. A. D. , Waheed, F. , Gunoglu, K. & Akkurt, İ. (2022). Experimental Testing of the Radiation Shielding Properties for Steel . International Journal of Computational and Experimental Science and Engineering , 8 (3) , 74-76 . DOI: 10.22399/ijcesen.1067028

25. Boodaghi Malidarre, R., Akkurt, I. Monte Carlo simulation study on TeO2–Bi2O–PbO–MgO–B2O3 glass for neutron-gamma 252Cf source. J Mater Sci: Mater Electron (2021). https://doi.org/10.1007/s10854-021-05776-y
26. Recep Kurtulus,Taner Kavas, Iskender Akkurt, Kadir Gunoglu. 2020. *Ceramics International* **46:**21120-21127. https://doi.org/10.1016/j.ceramint.2020.05.188
27. Al-Obaidi S., H. Akyıldırım, K. Gunoglu, I. Akkurt . 2020 *Acta Physica Polonica* A **137**. 551 DOI: 10.12693/APhysPolA.137.551
28. Akkurt I.,H. Akyıldırım, B. Mavi, S. Kilincarslan, C. Basyigit. 2010. *Ann. Nucl. Energy*. **37-7**. 910-914 DOI: 10.1016/j.anucene.2010.04.001
29. Günay, O. , Gündoğdu, Ö. , Demir, M. , Abuqbeitah, M. , Yaşar, D. , Aközcan, S. , Kapdan, E. & Yarar, O. (2019). Determination of the Radiation Dose Level in Different Slice Computerized Tomography . International Journal of Computational and Experimental Science and Engineering , 5 (3) , 119-123 . DOI: 10.22399/ijcesen.595645
30. Akkurt, I., Basyigit, C., Kilincarslan, S., Mavi, B., & Akkurt, A. 2006. *Cement and Concrete Composites,* **28:** 153-157. https://doi.org/10.1016/j.cemconcomp.2005.09.006
31. A.M.El-Khayatt, İ.Akkurt 2013. *Annals of Nuclear Energy*.**60:**8-14. https://doi.org/10.1016/j.anucene.2013.04.021
32. Günay, O. , Sarıhan, M. , Abamor, E. & Yarar, O. (2019). Environmental Radiation Doses from Patients Undergoing Tc-99m DMSA Cortical Renal Scintigraphy . International Journal of Computational and Experimental Science and Engineering , 5 (2) , 86-93 . DOI: 10.22399/ijcesen.589267
33. Huseyin Ozan Tekin, Baris CAVLI, Elif Ebru ALTUNSOY, Tugba MANICI, Ceren OZTURK, Hakki Muammer KARAKAS “An Investigation on Radiation Protection and Shielding Properties of 16 Slice Computed Tomography (CT) Facilities “International Journal of Computational and Experimental Science and Engineering 4-2(2018)37 – 40. https://doi.org/10.22399/ijcesen.408231
34. E.E. Altunsoy, H.O. Tekin, A. Mesbahi, I. Akkurt. 2020. *Acta Physica Polonica* A **137:**561. DOI: 10.12693/APhysPolA.137.561
35. I.Akkurt, A.M.El-Khayatt. 2013 *Annals of Nuclear Energy* **51**:5-9 https://doi.org/10.1016/j.anucene.2012.08.026
36. Caymaz, T. , Çalışkan, S. & Botsalı, A. R. (2022). Evaluation of Ergonomic Conditions using Fuzzy Logic in a Metal Processing Plant . International Journal of Computational and Experimental Science and Engineering , 8 (1) , 19-24 . DOI: 10.22399/ijcesen.932994
37. Iskender AKKURT, Huseyin Ozan TEKIN 2020.*Emerging Materials Research* **9:** https://doi.org/10.1680/jemmr.20.00209
38. I.Akkurt, H.Akyıldırım. 2012. *Nuclear Engineering and Design* **252:**163-166. https://doi.org/10.1016/j.nucengdes.2012.07.008
39. Ural, A. & Kilimci, Z. H. (2021). The Prediction of Chiral Metamaterial Resonance using Convolutional Neural Networks and Conventional Machine Learning Algorithms . International Journal of

Computational and Experimental Science and Engineering , 7 (3) , 156-163 . DOI: 10.22399/ijcesen.973726

40. Akkurt, I., Boodaghi Malidarreh, P., Boodaghi Malidarre, R., 2021. Simulation and Prediction the Attenuation Behavior of the KNN-LMN Based Lead Free Ceramics by FLUKA Code and Artificial Neural Network (ANN)-Based Algorithm, Environ. Technol. 1-15.
41. Akkurt, I., Waheed, F., Akyildirim, H., Gunoglu, K., 2020. Monte Carlo Simulation of a NaI(Tl) Detector Efficiency, J. radiat. Phys. Chem. https://doi.org/10.1016/j.radphyschem.2020.109081.
42. Abouhaswa, A. S., Zakaly, H. M., H., Issa, Shams A.M., Rashad, M., Pyshkina, M., Tekin, H.O., El-Mallawany, R., Mostafa, Y. A. M., 2021. Synthesis, Physical, Optical, Mechanical, and Radiation Attenuation Properties of TiO_2–Na_2O–Bi_2O_3–B_2O_3 Glasses, Ceram. Int. 47, 185–204.
43. Zarkooshi, A. , Latıf, K. H. & Hawı, F. (2021). Estimating the Concentrations of Natural Isotopes of 238 U and 232Th and Radiation Dose Rates for Wasit Province-Iraq by Gr-460 system . International Journal of Computational and Experimental Science and Engineering , 7 (3) , 128-132 . DOI: 10.22399/ijcesen.891935
44. E. Al-Sarraya, İ. Akkurt, K. Günoğlu, A. Evcin and N.Ç. Bezir. “Radiation Shielding Properties of Some Composite Panel” Acta Physica Polonica A 132-3(2017)490 DOI: 10.12693/APhysPolA.132.490
45. Albıdhanı, H. , Gunoglu, K. & Akkurt, İ. (2019). Natural Radiation Measurement in Some Soil Samples from Basra oil field, IRAQ State . International Journal of Computational and Experimental Science and Engineering , 5 (1) , 48-51 . DOI: 10.22399/ijcesen.498695
46. Nilgün Demir, Ayşe Kıvrak, Mahmut Üstün, Alp Cesur, İsmail Boztosun “Experimental Study for the Energy Levels of Europium by the Clinic LINAC” International Journal of Computational and Experimental Science and Engineering 3-1(2017)47-49
47. Kadir Gunoglu, Hatice Varol Özkavak, İskender Akkurt “Evaluation of gamma ray attenuation properties of boron carbide (B4C) doped AISI 316 stainless steel: Experimental, XCOM and Phy-X/PSD database software” Materials Today Communications. 29 (2021)102793. https://doi.org/10.1016/j.mtcomm.2021.102793
48. Jawad, A.A., Demirkol, N., Gunoğlu, K. et al. Radiation shielding properties of some ceramic wasted samples. Int. J. Environ. Sci. Technol. 16, 5039–5042 (2019). https://doi.org/10.1007/s13762-019-02240-7
49. Akkurt, I Basyigit C., Kilincarslan S., Beycioglu, A. Prediction of photon attenuation coefficients of heavy concrete by fuzzy logic. Journal of the Franklin Institute-Engineering and Applied Mathetamics. 347-9 (2010)1589-1597. DOI: 10.1016/j.jfranklin.2010.06.002
50. I. Akkurt, H. Akyıldırım, F. Karipçin, B. Mavi, “Chemical corrosion on gamma-ray attenuation properties of barite concrete,” Journal of Saudi Chemical Society,16-2 (2012) 199-202. https://doi.org/10.1016/j.jscs.2011.01.003
51. Ghada ALMisned, Duygu Sen Baykal, G. Susoy ,Gokhan Kilic, Hesham M.H. Zakaly, Antoaneta Ene, H.O. Tekin " Determination of gamma-ray transmission factors of WO3–TeO2–B2O3 glasses using

MCPX Monte Carlo code for shielding and protection purposes" Applied Rheology, vol. 32, no. 1, 2022… DOI: 10.1515/arh-2022-0132

52. Iskender Akkurt 2007. Effective Atomic Numbers for Fe–Mn Alloy Using Transmission Experiment Chinese Phys. Lett. 24 2812. https://doi.org/10.1088/0256-307X/24/10/027
53. Alsaif, N. A. M., Alotiby, M., Hanfi, M. Y., Mahmoud, K. A., Al Yousef, H. A., Alotaibi, B. M., Sayyed, M. I., Al-Hadeethi, Y., 2021. Comprehensive Study of Radiation Shielding and Mechanical Features of Bi_2O_3-TeO_2-B_2O_3-GeO_2 Glasses, J. Aust. Ceram. Soc. 57, 1267–1274.
54. Boodaghi Malidarre, R., Akkurt, I., 2022. The Influence of Nd_2O_3 on the Radiation Shielding, Physical, Mechanical, and Acoustic Properties of the (75-x) TeO_2 -15 MgO -10Na_2O -x Nd_2O_3 Glasses as a Potent Radiation Shielding Material, Polym. Compos. 43, 5418-5425.
55. Issa, S.A.M., Rashad, M., Zakaly, H. M. H., Tekin, H. O., Abouhaswa, A. S., 2020. Nb_2O_5-Li_2O-Bi_2O_3-B_2O_3 novel glassy system: evaluation of optical, mechanical, and gamma shielding parameters, J. Mater. Sci. Mater. Electron. 31, 22039-22056.
56. Makishima, A., Mackenzie, J. D., 1975. Calculation of Bulks Modulus, Shear Modulus and Piosson's Ratio of Glass J. Non-Cryst. Solids. 17, 147–157.
57. Makishima, A., Mackenzie, J. D., 1973. Direct Calculation of Young's Modulus of Glass, J. Non-Cryst. Solids. 12, 1973, 35–45.
58. Luo, J. P., Jia, X., Zheng, D. L., Wang, G., Sun, J. F., Yan, M., 2019. A Novel Approach to Achieving a Low Young's Modulus in Titanium-Based Metallic Glasses. J. Emerg. Mater. Res. 8, 22–28. https://doi.org/10.1680/jemmr.16.00098.
59. Inaba, S., Fujino, S., Morinaga, K., 1999. Young's Modulus and Compositional Parameters of Oxide Glasses, J. Am. Ceram. Soc. 82, 3501–3507.
60. Ahmadi, M., Zanganeh, V., Boodaghi Malidarre, R., Akkurt, I., 2022. Radiation Shielding, Physical, and Elastic Properties of BaO-B_2O_3-Bi_2O_3 Glass System, Phys. Scr. 97, 105309.
61. Boodaghi Malidarre, R., Akkurt, I., Ekmekci, I., Zakaly, H. M. H., Mohammed, H., 2022. The Role of La_2O_3 Rare Earth (RE) Material in the Enhancement of the Radiation Shielding, Physical, Mechanical and Acoustic Properties of the Tellurite Glasses, J. Radiat. Eff. Defects Solids, 1-13.
62. Ilik, E., Kilic, G., Issever, U. G., Issa, S. A. M., Zakaly, H. M. M., Tekin, H. O., Cerium (IV) Oxide Reinforced Lithium-Borotellurite Glasses: A Characterization Study Through Physical, Optical, Structural and Radiation Shielding Properties, Ceram. Int. 48, 1152-1165.
63. ALMisned, G., Zakaly, H. M. H., Issa, S. A. M., Ene, A., Kilic, G., Bawazeer, O., Almatar, A., Shamsi, D., Rabaa, E., Sideig, Z., Tekin, H. O., 2021. Gamma-Ray Protection Properties of Bismuth-Silicate Glasses against Some Diagnostic Nuclear Medicine Radioisotopes: A Comprehensive Study, Mater.14, 6668.
64. Kayiran, H. F., Akkurt, I., Boodaghi Malidarre, R., Kulali, F., 2022. The Effect of Nd_2O_3 on the Gamma-Neutron Shielding Properties for Iron-Boron-Phosphate Composites, J. Aust. Ceram. Soc. 1-7.

65. Malidarre, R.B., Akkurt, I. Simulation of neutron and gamma radiation shielding properties of KNN-LMN lead-free relaxor ceramics. J Aust Ceram Soc 59, 137–143 (2023). https://doi.org/10.1007/s41779-022-00819-x
66. Aktas, B., Acikgoz, A., Yilmaz, D., Yalcin, S., Dogru, K., Yorulmaz, N., 2022. The Role of TeO_2 Insertion on the Radiation Shielding, Structural and Physical Properties of Borosilicate Glasses, J. Nucl. Mater. 563, 153619.
67. Kashif, I., Abd El-Maboud, A., Ratep, A., 2014. Effect of Nd_2O_3 Addition on Structure and Characterization of Lead Bismuth Borate Glass, J. Results Phys. 4, 1–5.
68. Nazrin, S.N., Halimah, M.K., Muhammad, F.D., Yip, J.S., Hasnimulyati, L., Faznny, M. F., Hazlin, M.A.,, Zaitizila, I., 2018. The Effect of Erbium Oxide in Physical and Structural Properties of Zinc Tellurite Glass System, J. Non Cryst. Solids 490, 35–43.
69. Safiddine, S., Amokrane, K., Debieb, F., Soualhi, H., Benabed, B. & Kadri, E. (2021). How quarry waste limestone filler affects the rheological behavior of cement-based materials. Applied Rheology, 31(1), 63-75. https://doi.org/10.1515/arh-2020-0118
70. İ. Akkurt , S. Emikönel , F. Akarslan , K. Günoğlu , Ş. Kilinçarslan and İ.S. Üncü. “Barite Effect on Radiation Shielding Properties of Cotton–Polyester Fabric ” Acta Physica Polonica A 128-2B(2015)B53-B54 DOI: 10.12693/APhysPolA.128.B-53
71. Ghada ALMisned, Duygu Sen Baykal, Gokhan Kilic, G. Susoy, Hesham M.H. Zakaly, Antoaneta Ene, H.O. Tekin " Assessment of the usability conditions of Sb2O3-PbO-B2O3 glasses for shielding purposes in some medical radioisotope and a wide gamma-ray energy spectrum" Applied Rheology, vol. 32, no. 1, 2022 DOI: 10.1515/arh-2022-0133
72. Oruncak Bekir " Gamma-ray Shielding Properties of Nd2O3 added Iron-Boron-Phosphate based composites" Open Chemistry, vol. 20, no. 1, 2022. https://doi.org/ 10.1515/chem-2022-0143
73. Tan, T., Zhao, Y., Zhao, X., Chang, L. & Ren, S. (2022). Mechanical properties of sandstone under hydro-mechanical coupling. Applied Rheology, 32(1), 8-21. https://doi.org/10.1515/arh-2022-0120
74. Iskender Akkurt "Effective atomic and electron numbers of some steels at different energies" Ann. Nucl. En. 36-11,12(2009)1702-1705 DOI: 10.1016/j.anucene.2009.09.005
75. Kadir Gunoglu, İskender Akkurt “Radiation shielding properties of concrete containing magnetite, Progress in Nuclear Energy”137(2021)103776. https://doi.org/10.1016/j.pnucene.2021.103776

Figures

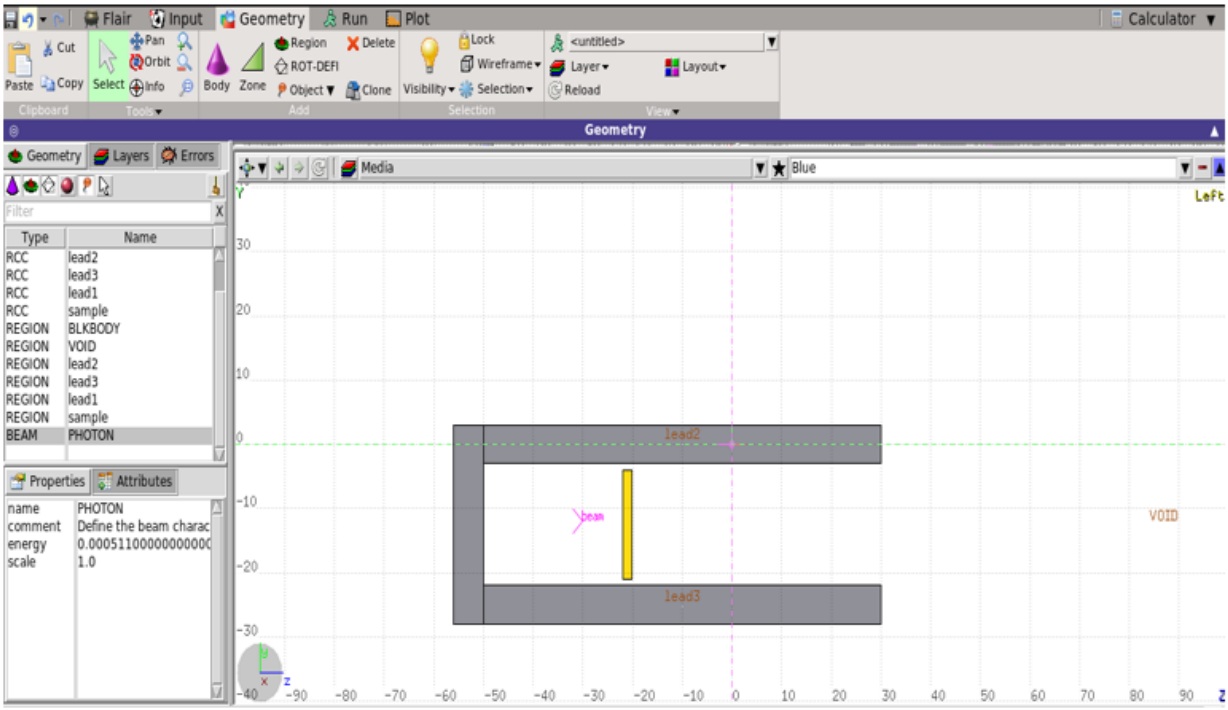

Figure 1

Screenshot of Flair interface for a left view of the simulation.

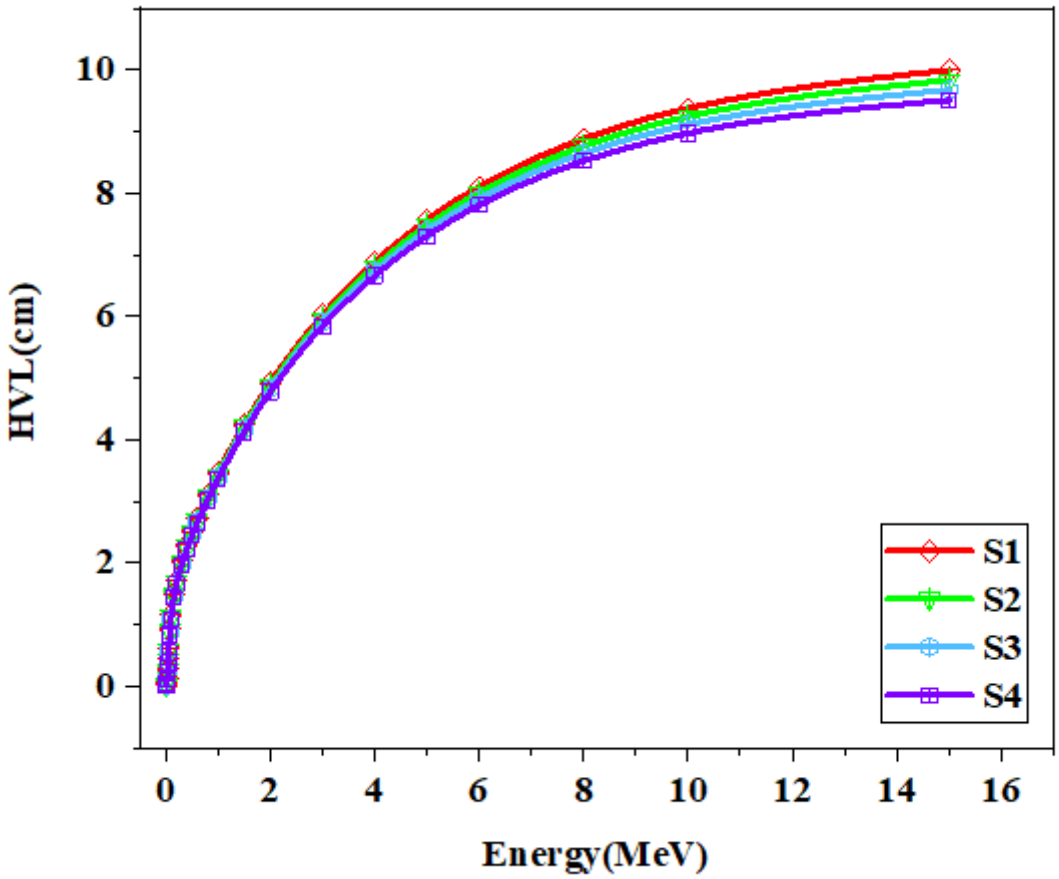

Figure 2

HVL versus initial gamma photon energy ranging from 0.01 to 15 MeV.

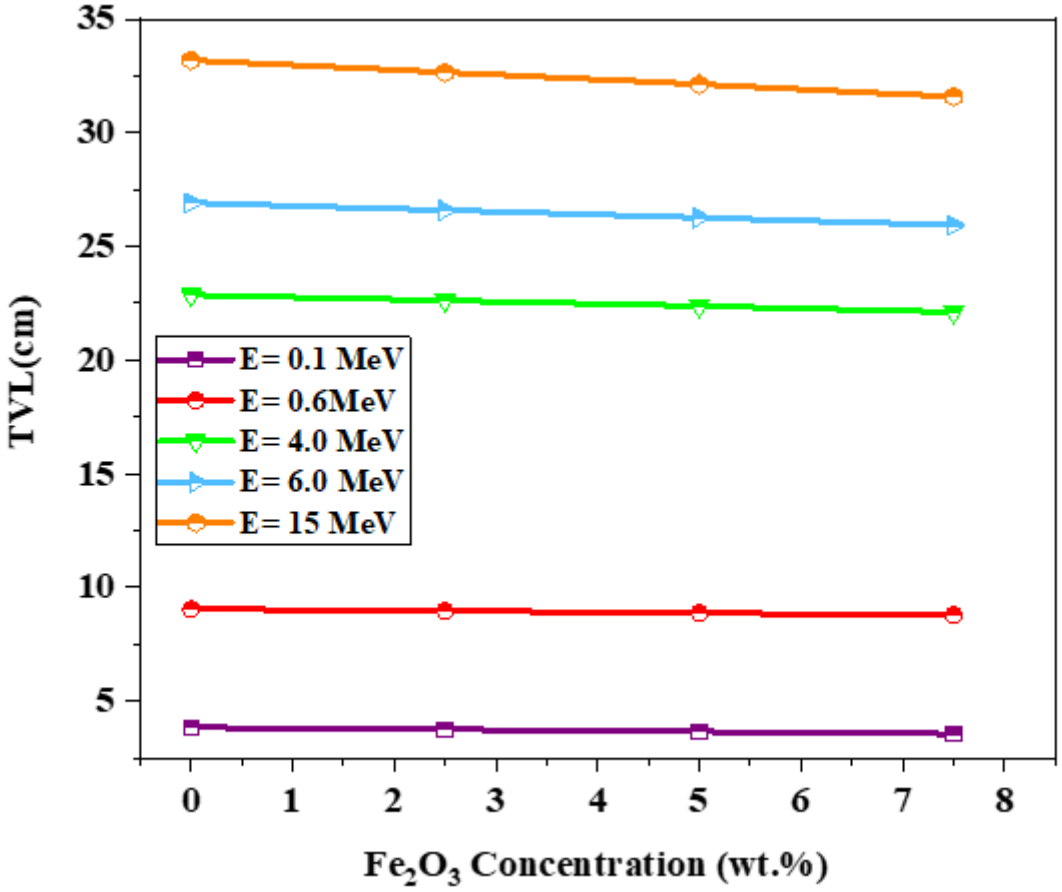

Figure 3

TVL versus Fe_2O_3 concentrations for 0.1, 0.6, 4.0, 6.0, and 15 MeV energy levels.

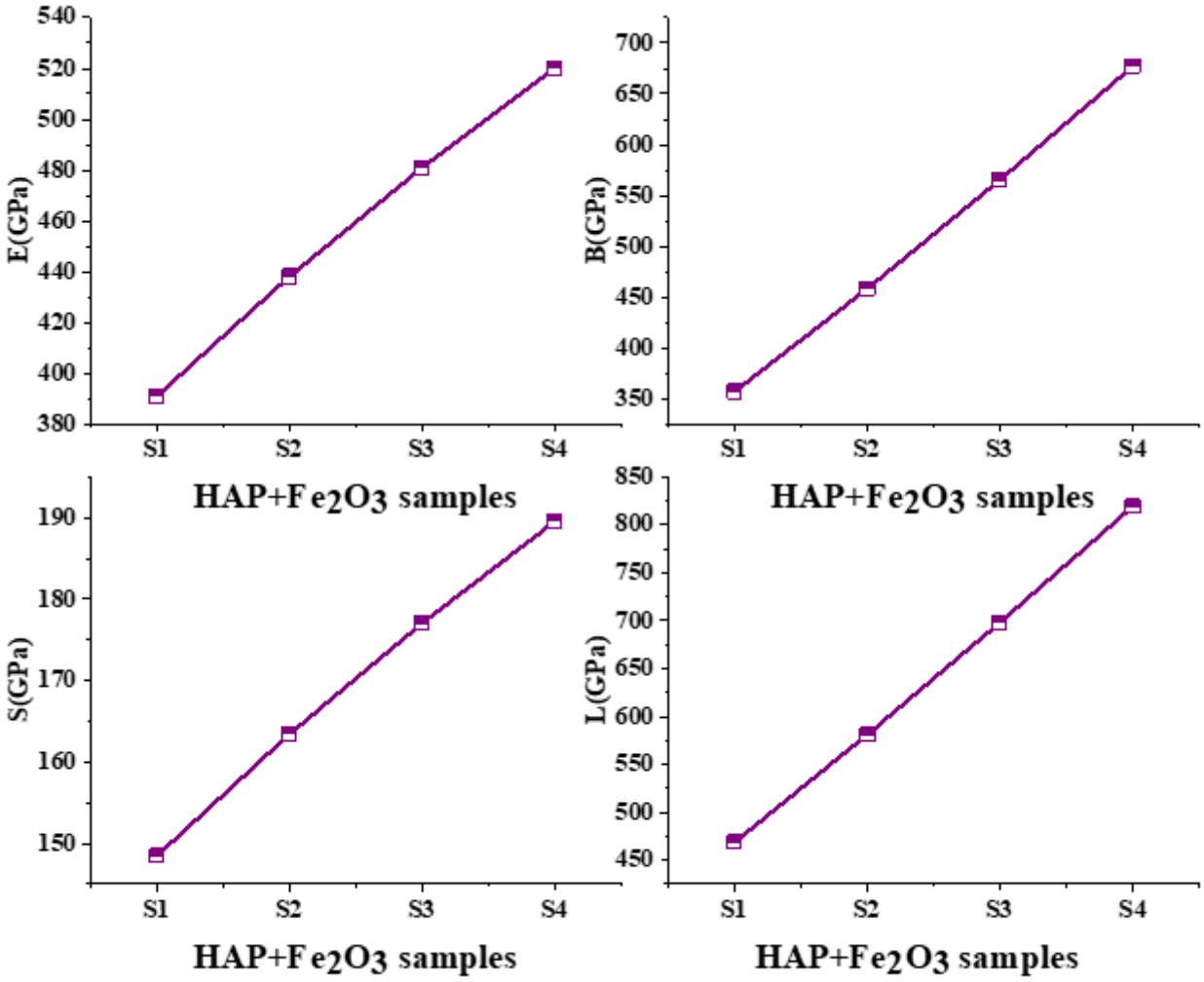

Figure 4

Mechanical moduli versus HAP+ Fe_2O_3 concentration.

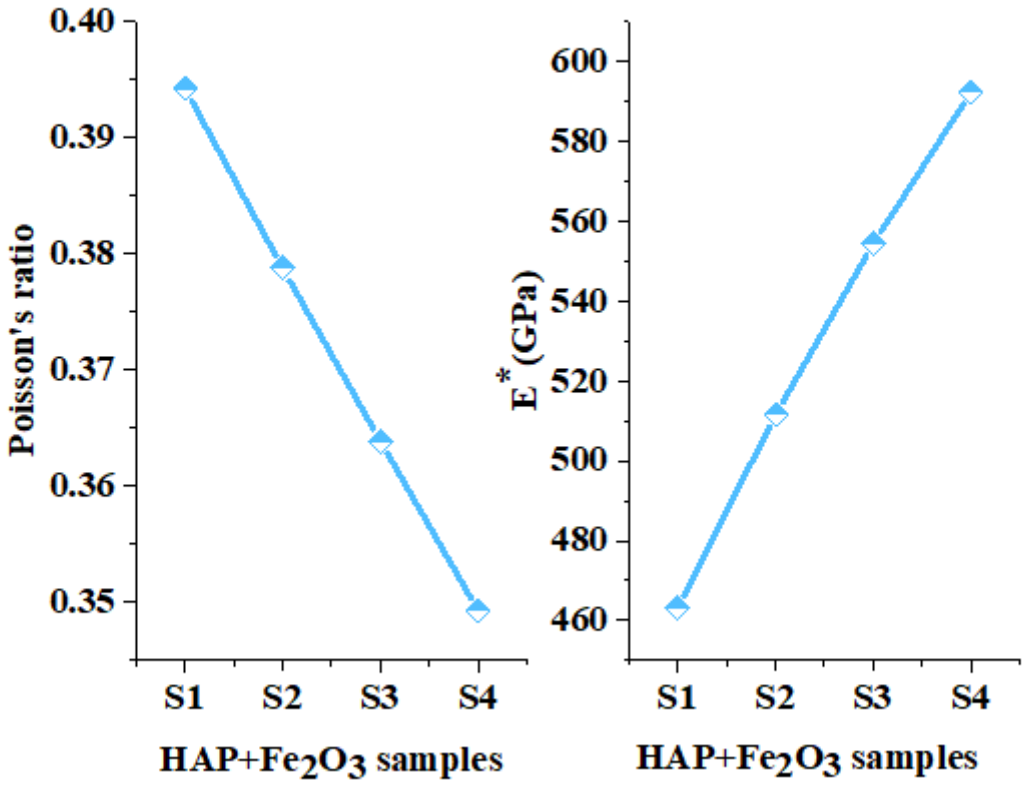

Figure 5

Poisson's ratio and E* versus HAP+ Fe_2O_3 concentration.

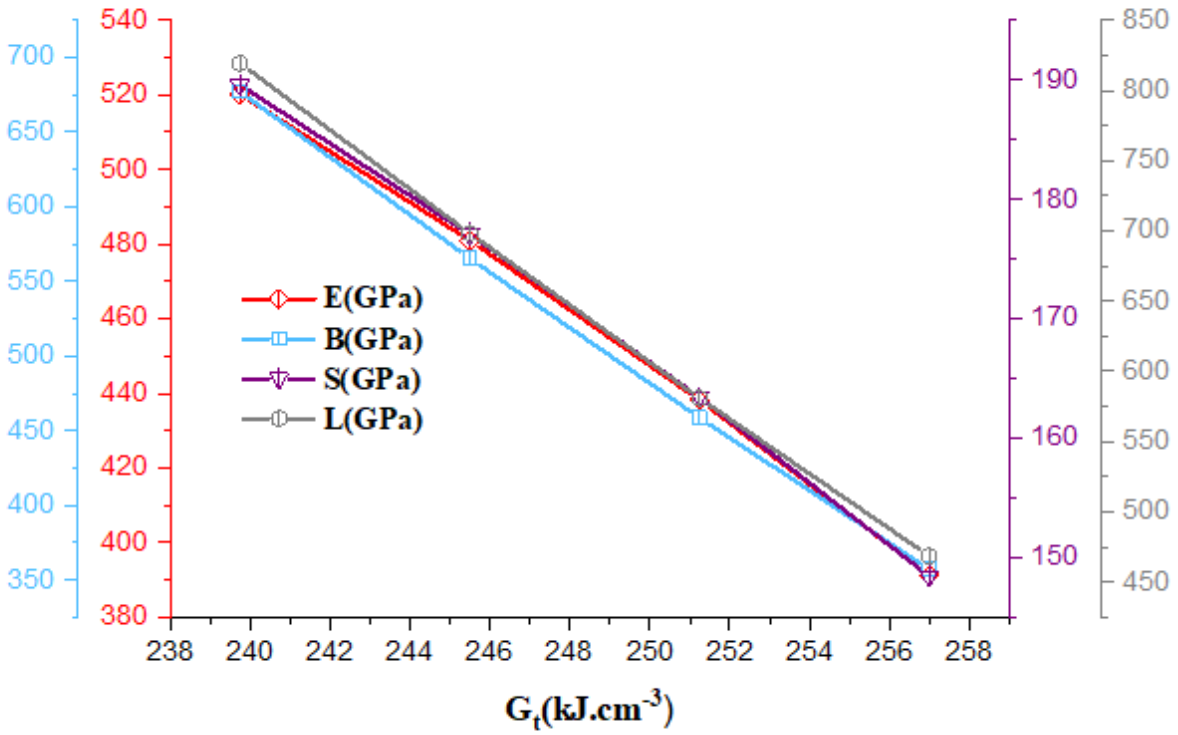

Figure 6

Mechanical moduli versus G_t.

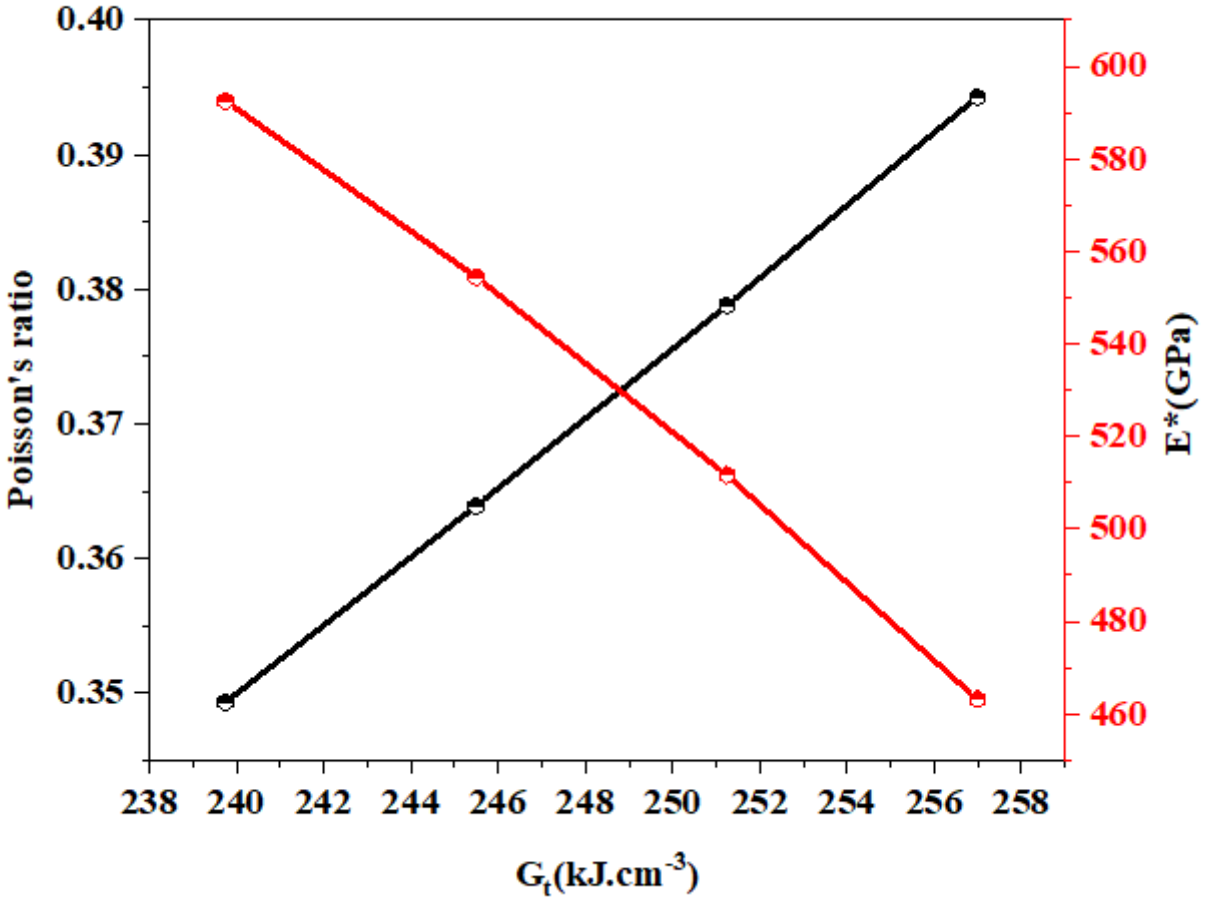

Figure 7

Poisson's ratio and E* versus G_t.

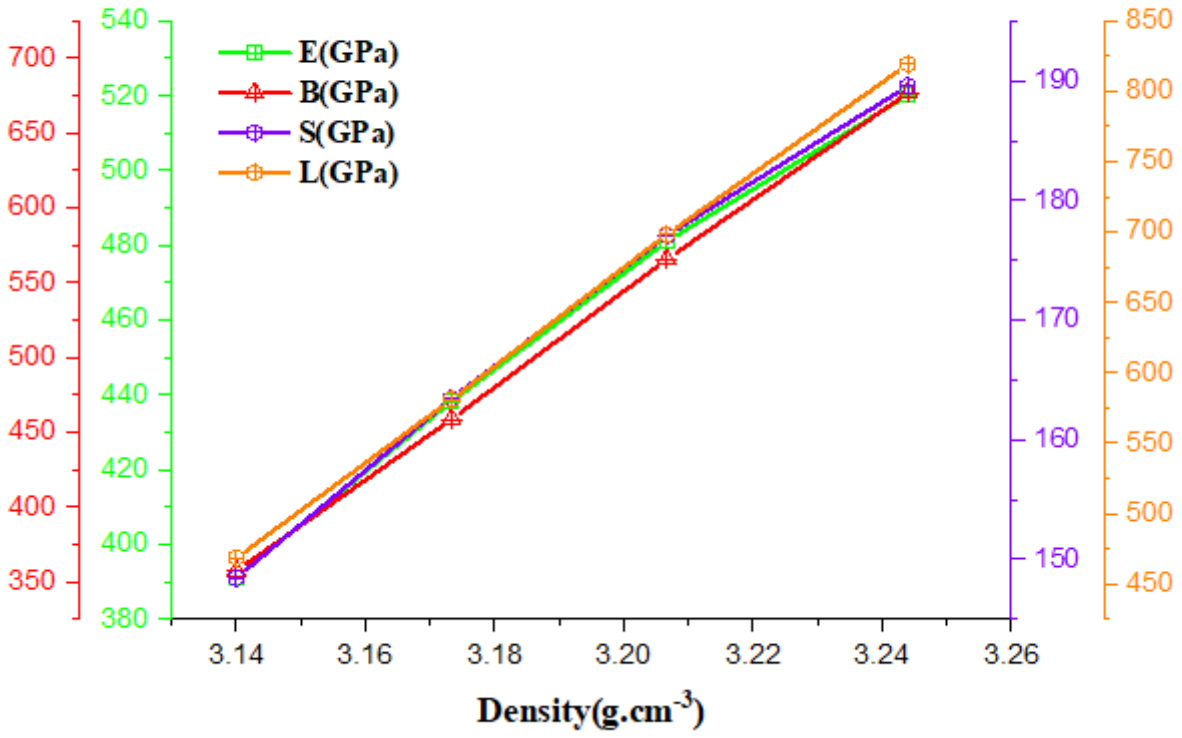

Figure 8

Mechanical moduli versus Density.

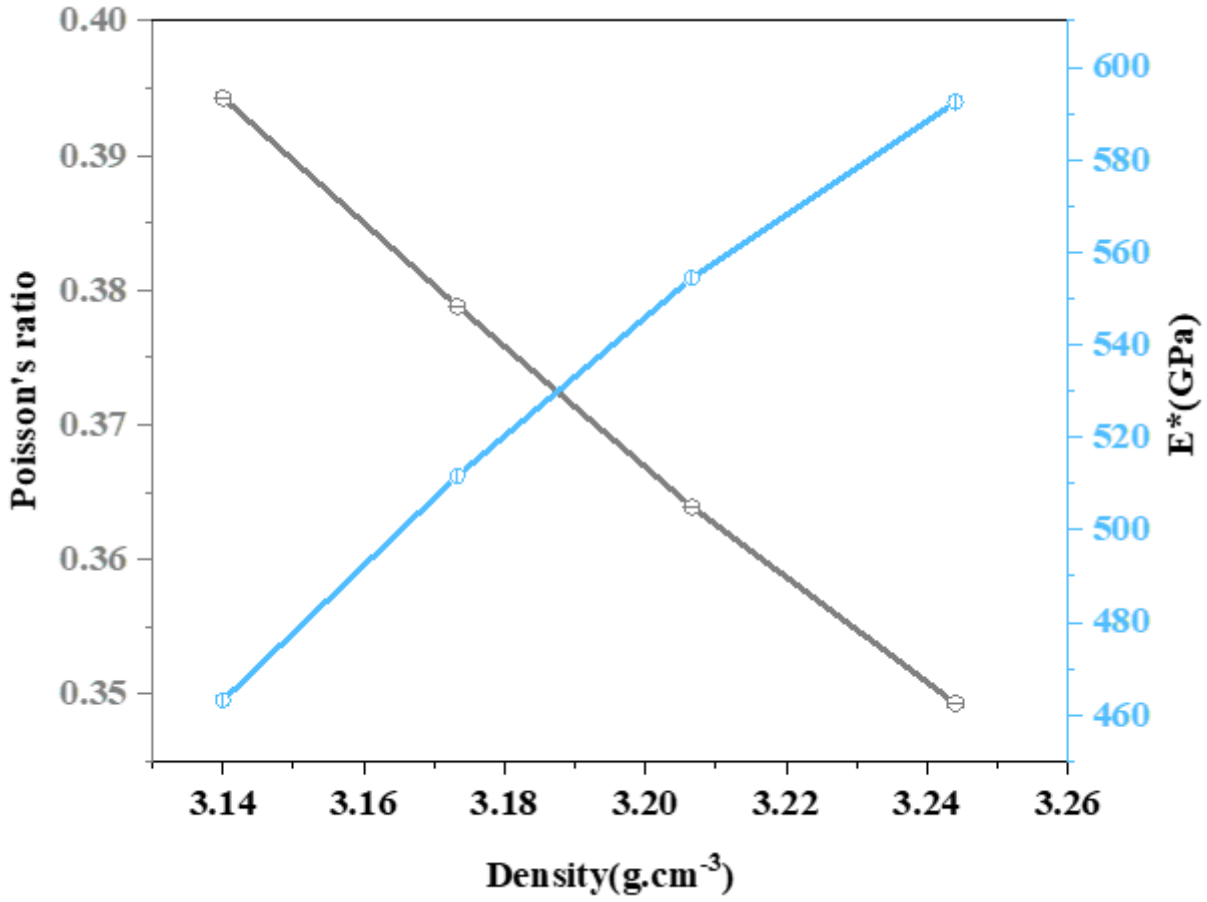

Figure 9

Poisson's ratio and E* versus density.

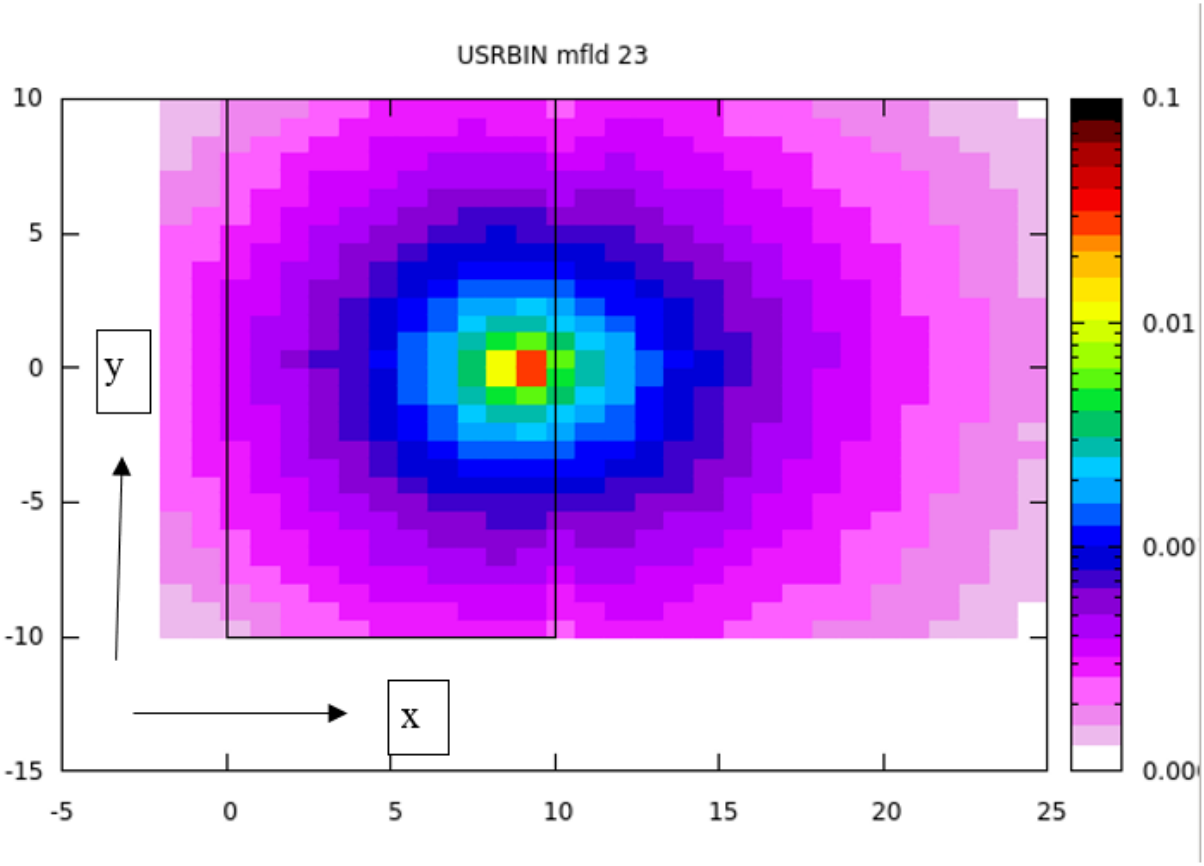

Figure 10

Charged particles' spatial map in the absence of the magnetic field for preferred composite.

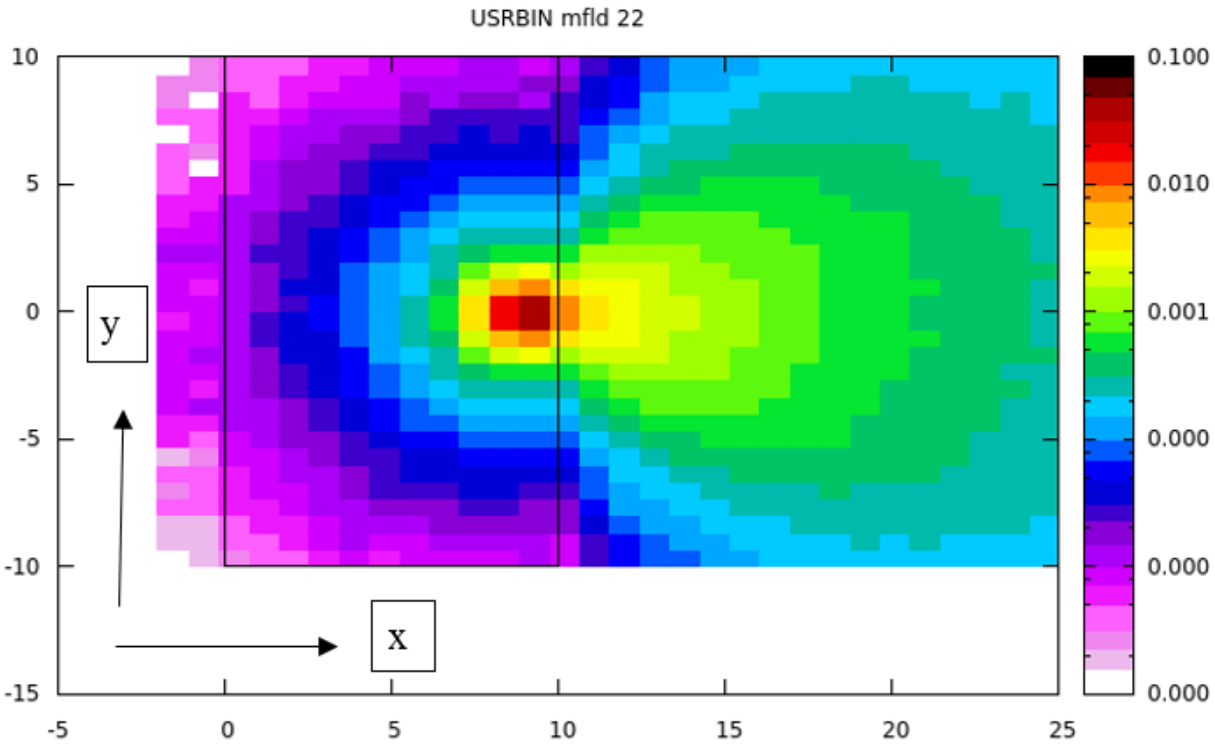

Figure 11

Charged particles' spatial map in the presence of the magnetic field (B_x=5 micro T) for preferred composite.